

Spectrally resolved fluorescence lifetime imaging microscopy: Förster resonant energy transfer global analysis with a one- and two-exponential donor model

Daniela Strat,^a Frank Dolp,^a Bjorn von Einem,^b Cornelia Steinmetz,^b Christine A. F. von Arnim,^b and Angelika Rueck^a

^aUniversity of Ulm, Institut für Lasertechnologien in Medizin, Helmholtzstrasse 12, Ulm, Baden-Württemberg 89081 Germany

^bUniversity of Ulm, Department of Experimental Neurology, 89081 Ulm, Germany

Abstract. In many fields of life science, visualization of spatial proximity, as an indicator of protein interactions in living cells, is of outstanding interest. A method to accomplish this is the measurement of Förster resonant energy transfer (FRET) by means of spectrally resolved fluorescence lifetime imaging microscopy. The fluorescence lifetime is calculated using a multiple-wavelength fitting routine. The donor profile is assumed first to have a monoexponential time-dependent behavior, and the acceptor decay profile is solved analytically. Later, the donor profile is assumed to have a two-exponential time-dependent behavior and the acceptor decay profile is derived analytically. We develop and apply a multispectral fluorescence lifetime imaging microscopy analysis system for FRET global analysis with time-resolved and spectrally resolved techniques, including information from donor and acceptor channels in contrast to using just a limited spectral data set from one detector only and a model accounting only for the donor signal. This analysis is used to demonstrate close vicinity of β -secretase (BACE) and GGA1, two proteins involved in Alzheimer's disease pathology. We attempt to verify if an improvement in calculating the donor lifetimes could be achieved when time-resolved and spectrally resolved techniques are simultaneously incorporated. © 2011 Society of Photo-Optical Instrumentation Engineers (SPIE). [DOI: 10.1117/1.3533318]

Keywords: Förster resonant energy transfer; global analysis; spectral fluorescence lifetime imaging microscopy; time-correlated single-photon counting.

Paper 10412R received Jul. 21, 2010; revised manuscript received Nov. 24, 2010; accepted for publication Dec. 7, 2010; published online Feb. 10, 2011.

1 Introduction

When and where do two proteins come into close proximity in living cells? These are key questions in many biological research projects. By exploiting Förster resonant energy transfer (FRET), the distance between two proteins that have been labeled with appropriate donor and acceptor fluorophores can be measured. When both fluorophores are in close vicinity (<10 nm), the donor transmits part of its excitation energy to the acceptor.¹ As a result, the intensity and lifetime of the donor fluorophore are decreased, whereas the intensity of the acceptor emission is increased.

FRET is dependent on the distance to the sixth power between the donor and the acceptor molecules and does not occur if this distance is >10 nm. Therefore, FRET between a donor and an acceptor molecule provides powerful high-quality information about the structure, dynamics, distance, and interactions of different species of biomolecules.² FRET analysis methods have also been used for the calculation of free-energy surface for protein folding.³ In the field of Alzheimer's disease (AD), it has been widely used to establish protein-protein interaction and also protein conformation.^{4–8} However, FRET measurements and analysis in living cells is very challenging due to suboptimal excitation and emission overlap of donor and acceptor,

high autofluorescence, low quantum yield of living color tags, reduced signal intensity of proteins with low abundance, and hence, poor signal-to-noise (S/N) ratio. A very complex situation arises when more than one compound has to be analyzed. This could be the case when endogenous fluorophores of living cells and tissues have to be discriminated to identify oxidative metabolic changes.⁹

A widely accepted method to analyze FRET is fluorescence lifetime imaging microscopy (FLIM)^{10,11} by spatially resolving the lifetimes of the interacting molecular species. Historically, FRET was primarily analyzed from data of the donor lifetimes measured by one detector (with a narrow spectral region only).

Data measured simultaneously, at more than one spectral region, is the basis of multispectral FLIM or spectral FLIM (SLIM).^{11–15} The information content can be richer when the spectrally resolved data are simultaneously analyzed. Parameters such as the concentration of interacting species and the lifetimes of the donors and acceptors are invariant across all the measured channels, thus making global analysis^{16–21} a potent method that offers better estimation of the required parameters.

SLIM is working in the time domain employing excitation with short light pulses and detection of the fluorescence intensity decay in many cases with time-correlated single-photon counting (TCSPC). Spectrally resolved detection is achieved by a polychromator in the detection path and a 16-channel multi-anode photomultiplier tube (PMT) with the appropriate routing electronics.²²

Address all correspondence to: Angelika Rueck and Daniela Strat, University of Ulm, Institut für Lasertechnologien in Medizin, Helmholtzstrasse 12, 89081 Ulm, Germany. Tel: 0049731 142916; E-mail: angelika.rueck@ilm.uni-ulm.de and E-mail: danastrat@yahoo.com.

This paper discusses various possibilities that SLIM and global analysis offer for improving molecular imaging in living cells, as well as successfully realized applications. Special attention is focused on FRET measurements with respect to protein interactions involved in processing of β -amyloid (A β) precursor protein (APP).^{6,7} APP is cleaved sequentially by β -site of APP-cleaving enzyme (BACE) and γ -secretase to release the A β peptides that accumulate in plaques in AD. GGA1, a member of the Golgi-localized γ -ear-containing ARF-binding (GGA) protein family, interacts with BACE and influences its subcellular distribution. Here, we extended previous work using BACE and GGA1 tagged with fluorescent proteins as a FRET pair in living cells. FRET calculations are improved using novel, global analysis data-fitting algorithms taking into account the multidimensional datasets that result from the kinetic equations in every spectral channel.

2 Methodology

2.1 Experimental Setup

In order to investigate SLIM of different fluorophores (for example donor/acceptor pairs), a Ti:sapphire laser (Tsunami, Spectra Physics, Darmstadt, Germany) was coupled to a laser scanning microscope (LSM410, Carl Zeiss, Germany). The Tsunami laser is a mode-locked 82-MHz laser with a tuning range of 750–960 nm, a maximum optical output power of \sim 780 mW and a pulse width of $<$ 100 fs. For cellular studies, the power at the input of the microscope was reduced to 120 mW. This corresponds to an average irradiation of \sim 70 J/cm² with respect to the scanned sample plane and acquisition time of 8×8 s. Two-photon excitation was performed at 800 nm. The choice of 800 nm was established empirically to reduce cross-excitation of monomeric red fluorescent protein (mRFP) and autofluorescence.⁶

For SLIM, the fluorescence light from the second descanned detection channel of the LSM410 was coupled into a 600- μ m multimode fiber. The end of the fiber was put into the input focal plane of an MS125 spectrograph (LOT-Oriel). A PML-16 multichannel PMT module (Becker&Hickl GmbH, Berlin, Germany) was attached to the output of the spectrograph (see Fig. 1). The PML-16 contains a 16 channel Hamamatsu R5900–01-L16 multianode PMT and the TCSPC routing electronics.²² We used a grating of 600 lines/mm in the spectrograph. This grating yields a 200-nm spectral range spread over the 16 channels of the detector. The spectral bandwidth of the PMT channels is \sim 12.5 nm.

The principle of SLIM detection was described recently.^{14,15} Briefly, the PML-16 detector module delivers a timing pulse and a ‘channel’ signal for each individual photon. The signals are connected to the timing input and the routing input of an SPC-830 TCSPC module (Becker&Hickl GmbH, Berlin, Germany). Simultaneously, the SPC-830 module receives the scan clock pulses (frame sync, line sync, and pixel clock) from the scan controller of the LSM 410, which determines the spatial location of the signal.

For each photon, the TCSPC module determines the location within the scanning area, the time of the photon within the laser pulse period, and the detector channel number (i.e., the wavelength range). These parameters build up a three-

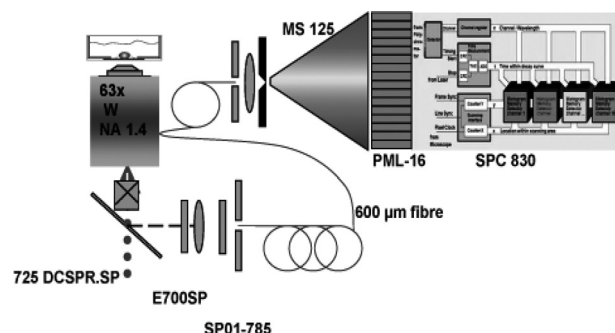


Fig. 1 Principal components of the SLIM apparatus.

dimensional photon distribution over the scan area, the wavelength, and the time in the fluorescence decay. For the results presented in section 3, we used an image size of 128×128 pixels, 64 time values, and 16 wavelength channels. An acquisition time of 8×8 s was used to record the data.

The microscope objective lens was a 63 \times magnification NA 1.2 water immersion lens (C-APO 63 \times , Carl Zeiss, Germany). A zoom factor of 2 gave a resolution of 0.5 μ m/pixel.

SLIM experiments have been performed over 16 channels, first for the control model made by human neuroblastoma (N2A) cells transfected with donor-EGFP molecules alone or N2A cells transfected with a mixture of donor-GFP and acceptor-mRFP molecules.

A similar set of SLIM experiments was performed for a model made by N2A cells transfected with GGA1-EGFP alone or cotransfected with GGA1-EGFP plus BACE-mRFP proteins. The emission profiles of the donor or acceptor molecules are wavelength dependent due to the wavelength dependency of the quantum yields, and they can have values close to zero for the wavelengths where they do not emit or emit very little. The experimental data were measured over 16 spectral channels covering the range between 450 and 650 nm (12.5 nm/channel). The fluorescence light intensity is recorded by photomultipliers on each of the 16 spectral channels and over 64 time points with 195-ps time resolution. The fluorescence lifetimes of the donor and acceptor and also various mixtures within the different spectral channels were calculated from the TCSPC raw data by using a multichannel global fitting algorithm that assumes a monoexponential as well as a two-exponential behavior for the donor.

2.1.1 Fluorophores

FRET was measured between the donor protein EGFP and the acceptor protein mRFP, widely accepted for the use in green/red pairs.^{8,23,24} Cells were cotransfected with the proteins tagged to EGFP or mRFP, respectively. For control experiments cells were transfected with EGFP or mRFP alone or with a tandem-protein consisting of EGFP and mRFP linked by a peptide of 7 amino acids. To detect proximity of GGA1 and BACE, N2A cells were transfected with GGA1-EGFP alone or cotransfected with GGA1-EGFP plus BACE-mRFP proteins.

2.1.2 Generation of expression constructs of GGA1 and BACE

GGA1 cDNA⁶ was transferred from GGA1-pcDNA3.1-myc into the multiple cloning site of the vector pEGFP-N3 (Clontech,

Mountain View, California) by using *NheI* and *XhoI* restriction sites. GGA1-pcDNA3.1-myc, EGFP, mRFP, EGFP-mRFP tandem, and BACE-mRFP have been described elsewhere.^{6,8,24} Authenticity was confirmed by deoxyribose nucleic acid (DNA) sequencing.

2.1.3 Cell culture

N2A human neuroblastoma cells were grown in Dulbecco's Modified Eagle Medium (DMEM) [Invitrogen (Gibco), Karlsruhe, Germany] medium supplemented with 10% fetal bovine serum and $1 \times$ penicillin/streptomycin at 37°C and 5% CO₂. For microscopy, all cells were seeded on glass-bottom microwell dishes, with coverglass 0.16–0.19 mm (MatTek Corporation, Ashland, MA 01721, USA) at a density of 10–25 cells/mm², and were allowed to grow for 24 h after transient transfection using Satisfaction (Agilent, Waldbronn, Germany), according to manufacturer's instructions. Microscopic observation was performed immediately after removing the incubation medium and rinsing twice with indicator free DMEM at 37°C.

2.1.4 Algorithms for global analysis

The data analysis was done using MATLAB, solving the nonlinear curve-fitting (data-fitting) problem in a least-squares sense using the routine "lsqcurvefit," which finds the vector of coefficients \mathbf{x} that solve the problem:

$$\begin{aligned} \min_{\mathbf{x}} \|F(\mathbf{x}, \mathbf{x} \text{ data}) - \mathbf{y} \text{ data}\|_2^2 \\ = \min_{\mathbf{x}} \sum_i [F(\mathbf{x}, \mathbf{x} \text{ data}_i) - \mathbf{y} \text{ data}_i]^2 \end{aligned}$$

given input data \mathbf{x} data, and the observed output \mathbf{y} data, where \mathbf{x} data and \mathbf{y} data are matrices or vectors of length m , and $F(\mathbf{x}, \mathbf{x} \text{ data})$ is a vector-valued function.

In our case, the \mathbf{x} data vector was the time data, the \mathbf{y} data vector was the fluorescence intensity data, and the vector of variable parameters contained all the donor and acceptor amplitudes for all the channels and all the donor and acceptor decay rates. The model was evaluated for each time point from the \mathbf{x} data, and each value of the experimental data was subtracted from the value of the model at each time point.

2.2 Spectrally Resolved Global Analysis of the Fluorescence Lifetime

Data recorded on more than one channel can have richer information content (if linearly independent from channel to channel) than a single channel, resulting in possibly improved FRET calculations when applying a global analysis routine. Donor and acceptor molecule species are found in a FRET experiment. Initially, the donors and acceptors are in the ground state. When light impinges onto the sample, the donor molecules begin being excited from the ground state. They are excited continuously until all are excited or until the light source is switched off. The time $t = 0$ is considered when the light source is switched off. The concentration of the initial excited donors at time $t = 0$ is D_0 and the concentration of excited donors at time t is $D^*(t)$. Three main mechanisms relax them to the ground state: (i) fluorescing light emission with a decay rate K_f^D , (ii) radiationless

decay with a decay rate K_{nl}^D , (iii) transferring their energy to the acceptor molecules with a decay rate K_{ET}^D .

The simplest case scenario is described by considering the donors to exhibit a single exponential behavior given in Eq. (1), with a decay rate given by the sum of the three decay rates considered above,

$$\frac{d[D^*(t)]}{dt} = -(K_f^D + K_{nl}^D + K_{ET}^D)[D^*(t)]. \quad (1)$$

At time $t = 0$, the concentration of the excited acceptor molecules is A_0 and, at time $t > 0$, is $A^*(t)$. The acceptor molecules start receiving energy from the donors with a rate K_{ET}^D until they all become excited or until all the available donor molecules have transferred their energy to the acceptors. The excited acceptors relax to the ground state through two main mechanisms: (i) fluorescing light emission with a decay rate K_f^A , (ii) radiationless decay with a decay rate K_{nl}^A , as shown in

$$\frac{d[A^*(t)]}{dt} = K_{ET}^D[D^*(t)] - (K_f^A + K_{nl}^A)[A^*(t)]. \quad (2)$$

The system of equations (1) and (2) was solved analytically for the time-dependent concentration of the excited donors and the time-dependent concentration of the excited acceptors, and the solution is shown as follows:

$$D^*(t) = D_0 e^{-(K_f^D + K_{nl}^D + K_{ET}^D)t}, \quad (3)$$

$$\begin{aligned} A^*(t) = \frac{K_{ET}^D D_0 [e^{-(K_f^A + K_{nl}^A)t} - e^{-(K_f^D + K_{nl}^D + K_{ET}^D)t}]}{(K_f^D + K_{nl}^D + K_{ET}^D) - (K_f^A + K_{nl}^A)} \\ + A_0 e^{-(K_f^A + K_{nl}^A)t}. \end{aligned} \quad (4)$$

In a first approximation, it was assumed that the acceptor molecules do not absorb light directly from the excitation light source, thus A_0 , the initial concentration of the excited acceptors, is practically zero: $A_0 = 0$.

An example of the theoretical profiles for the time-dependent concentrations of the excited donor and excited acceptor is given in Fig. 2. The fluorescence intensity signal, emitted by the excited donor molecules, with no acceptor present, for a particular emission wavelength λ , is given in Eq. (5). B^D is a proportionality constant that, for a particular wavelength λ , is the convolution of the instrument response, the quantum efficiency of the donor fluorophores, and the radiant power of the excitation source,

$$I^D(t, \lambda) = [B^D(\lambda)]D^*(t). \quad (5)$$

Replacing in Eq. (5) the concentration from Eq. (3) of the excited "disturbed" donors (i.e., when the acceptors are present), offers in Eq. (6) the detailed fluorescence signal intensity for the donor molecules, as follows:

$$I^D(t, \lambda) = [B^D(\lambda)]D_0 e^{-(K_f^D + K_{nl}^D + K_{ET}^D)t}. \quad (6)$$

The fluorescence signal intensity emitted by the acceptor molecules alone for a particular emission wavelength λ is given by Eq. (7). B^A is a proportionality constant that, for a particular wavelength λ , is the convolution of the instrument response, the quantum efficiency of the acceptor fluorophores, and the radiant power of the excitation source.

$$I^A(t, \lambda) = B^A(\lambda)[A^*(t)] \quad (7)$$

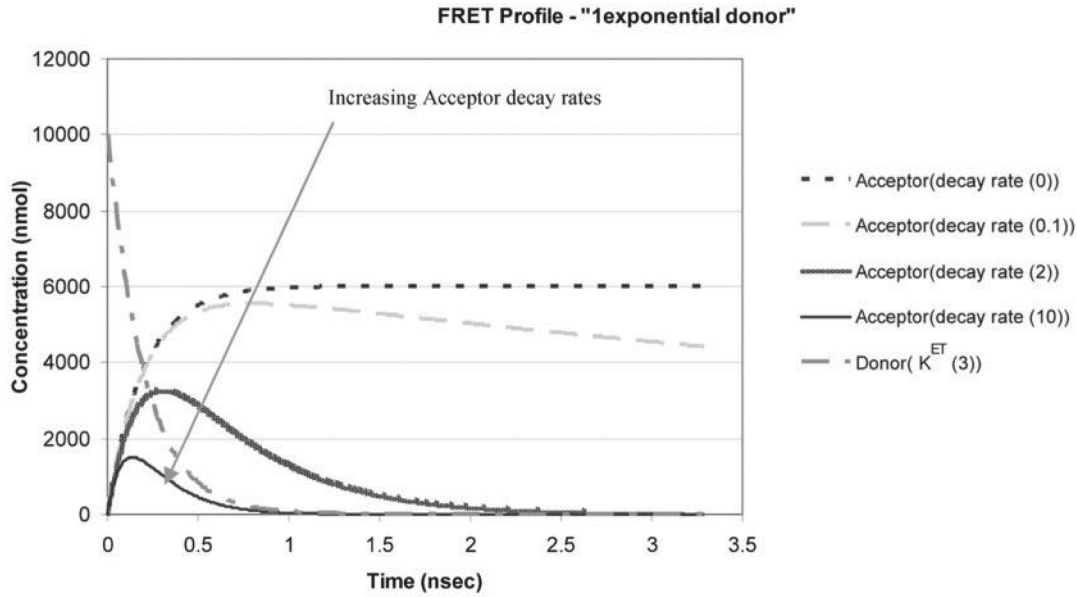


Fig. 2 Variation of excited donor and acceptor profiles versus time for a monoexponential behavior of the donor molecules for a FRET interaction with $K_f^D + K_n^D + K_{ET}^D = 5$; $K_{ET}^D = 3$; $D_0 = 10000$, and $K_f^A + K_n^A = 0, 0.1, 2, \text{ and } 10$.

Replacing in Eq. (7) the concentration from Eq. (4) of the excited acceptors, and considering the initial concentration of the excited acceptors $A_0 = 0$, offers in Eq. (8) the detailed fluorescence signal intensity for the acceptor molecules as follows:

$$I^A(t, \lambda) = B^A(\lambda) \frac{[K_{ET}^D D_0 (e^{-(K_f^A + K_n^A)t} - e^{-(K_f^D + K_n^D + K_{ET}^D)t})]}{[(K_f^D + K_n^D + K_{ET}^D) - (K_f^A + K_n^A)]} \quad (8)$$

For a mixture of donor and acceptor molecules under investigation, the fluorescent signal received at the detectors for any emission wavelength is a mixture of signals emitted by the fluorescing donors and fluorescing acceptor molecules.

The fluorescence intensity signal recorded for any emission wavelength λ , for a mixture of acceptor and donor molecules is given by

$$I(t, \lambda) = B^D(\lambda)D^*(t) + B^A(\lambda)A^*(t) \quad (9)$$

Replacing in Eq. (9) the concentration from Eq. (3) of the excited donors and from Eq. (4) of the excited acceptors, offers in Eq. (10) the detailed fluorescence signal intensity from the mixture of donor and acceptor molecules as follows:

$$I(t, \lambda) = B^D(\lambda)D_0 e^{-(K_f^D + K_n^D + K_{ET}^D)t} + B^A(\lambda) \frac{[K_{ET}^D D_0 (e^{-(K_f^A + K_n^A)t} - e^{-(K_f^D + K_n^D + K_{ET}^D)t})]}{[(K_f^D + K_n^D + K_{ET}^D) - (K_f^A + K_n^A)]} \quad (10)$$

The more complex case scenario is described by considering the donor in the presence of the acceptor to exhibit a two-exponential behavior, with one decay rate given in Eq. (1) and a second decay

rate K_2^D as shown as follows:

$$\frac{d[D^*(t)]}{dt} = -(K_f^D + K_n^D + K_{ET}^D)[D^*(t)] - K_2^D[D^*(t)]. \quad (11)$$

The donor molecules that are close enough to the acceptor molecules transfer their energy to the acceptor molecules with a decay rate K_{ET}^D . The donor molecules that would not be able to transfer their energy to the acceptor molecules relax to the ground state through only two mechanisms: (i) fluorescing light emission with a decay rate K_f^D , (ii) radiationless decay with a decay rate K_n^D . The second exponential in the donor model with a decay rate K_2^D is the decay rate of the donor molecules that would not transfer their energy to the acceptor molecules via intermolecular FRET and is given by the sum $K_2^D = K_n^D + K_f^D$.

The system of equations (11) and (2) was solved analytically for the time-dependent concentration of the excited donors and the time-dependent concentration of the excited acceptors, and the solution is shown in Eqs. (12) and (13), respectively,

$$D^*(t) = D_0 [C e^{-(K_f^D + K_n^D + K_{ET}^D)t} + (1 - C)e^{-K_2^D t}] \quad (12)$$

$$A^*(t) = C K_{ET}^D D_0 \frac{[(e^{-(K_f^A + K_n^A)t} - e^{-(K_f^D + K_n^D + K_{ET}^D)t})]}{[(K_f^D + K_n^D + K_{ET}^D) - (K_f^A + K_n^A)]} \quad (13)$$

It can be seen in Eq. (12) that for the “undisturbed” donors, when $K_{ET}^D = 0$, the decaying profile of the excited donors becomes single exponential. If there are enough acceptor molecules so that all are close enough to the donor molecules to interact via FRET, then the behavior of the excited donor molecules is also monoexponential ($C = 1$). Only the interacting “disturbed” donors that are close enough to the acceptor molecules are considered when finding the analytical solution [Eq. (13)] for the excited

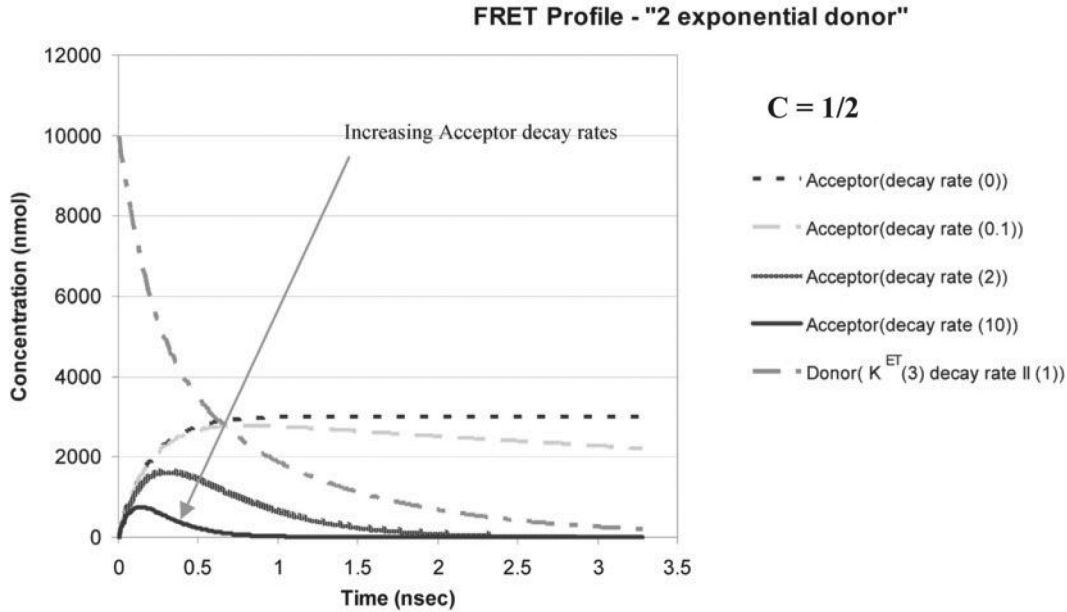


Fig. 3 Variation of excited donor and acceptor profiles versus time for a two-exponential behavior of the donor molecules for a FRET interaction with $K_f^D + K_{rl}^D + K_{ET}^D = 5$; $K_{ET}^D = 3$; $K_2^D = 2$; $D_0 = 10000$; $K_f^A + K_{rl}^A = 0, 0.1, 2, \text{ and } 10$.

acceptors. C is the fraction from the total number of donors that is able to interact with the acceptor molecules via FRET.

The fluorescence intensity signal recorded for any emission wavelength λ , for the acceptor and the “disturbed” donor molecules, is given in Eq. (9). When inserting Eqs. (12) and (13) in Eq. (9), we obtain the concentration profile for the two-exponential donor model. This is represented graphically in Fig. 3.

3 Results

Fitting the experimental data with the models shown in Eqs. (5) and (9) for both monoexponential [given by Eqs. (3) and (4)] and two-exponential donor models [given by Eqs. (12) and (13)], helps in retrieving the unknown variables: the donor decay rates K_f^D , K_{rl}^D , K_{ET}^D , the initial concentration of the excited donor D_0 , the acceptor decay rates K_f^A , K_{rl}^A , the donor amplitude coefficients for the different i channels $B^D(\lambda)_i$, and the acceptor amplitude coefficients for the different i channels $B^A(\lambda)_i$ with $i = 1-16$.

For the control cells, the experimental data of the donor alone (derived from a cell transfected only with EGFP) has shown highest intensity on channel 11 ($\lambda = 525-512.5$ nm). Channels 1-3 and 15-16 are noisier than channels 4-14 for donor-EGFP alone, so the fitting procedure was done for three different data sets: (i) A fitting routine of the donor signal alone was performed for channel 11, (ii) a global fitting for 11 channels (channel 4-14), and (iii) a global fitting for 16 channels (channel 1-16). For the donor-EGFP only model, the energy transfer rate was considered $K_{ET}^D = 0$ because of the lack of energy transfer in the absence of the acceptor.

The experimental data for the donor-acceptor: EGFP-mRFP were derived from a cell transfected with the protein EGFP-mRFP. Again, channels 1-3 and 15-16 are noisier than channels 4-14. The data from a mixture of acceptor-mRFP and donor-

EGFP have been fitted in the same manner: (i) for the strongest intensity channel (11) alone, (ii) for channels 4-14, and (iii) for channels 1-16, using a donor-acceptor model given in Eq. (10).

The minimization routine has been performed in two manners: (i) over all the parameters (i.e., all the decay rates and all the extinction coefficients of the donor and acceptor) and (ii) keeping some of the parameters constant (such as fluorescent and radiationless decay rates of the donor and the wavelength-dependent amplitudes of the donor for all the available channels) to the values for donor-EGFP alone (for 16 channels global fit), while performing the fitting routine with variable acceptor decay rates and the acceptor amplitude coefficients for all the available channels. For all minimization routines, the experimental data were extracted from a 3×3 pixel area (binning 1).

The values of the variable amplitudes and decay rates are summarized in Tables 1-3 for the donor-EGFP alone. The fit for the different channels is demonstrated in Fig. 4. The lifetime of the donor alone is defined as τ^D and is given as follows:

$$\tau^D = \frac{1}{K_f^D + K_{rl}^D} \quad (14)$$

The values of the fitted parameters for the donor-acceptor EGFP-mRFP model using a one-exponential donor are summarized in Tables 4-12. The lifetime of the donor in the presence of the acceptor is given as follows:

$$\tau^{DA} = \frac{1}{K_f^D + K_{rl}^D + K_{ET}^D}. \quad (15)$$

It can be seen that the lifetime of the donor in the presence of the acceptor is, in all cases, shorter than the lifetime of the donor when there is no acceptor—when using a donor model. The FRET efficiency is defined as:

$$E = 1 - \frac{\tau^{DA}}{\tau^D}. \quad (16)$$

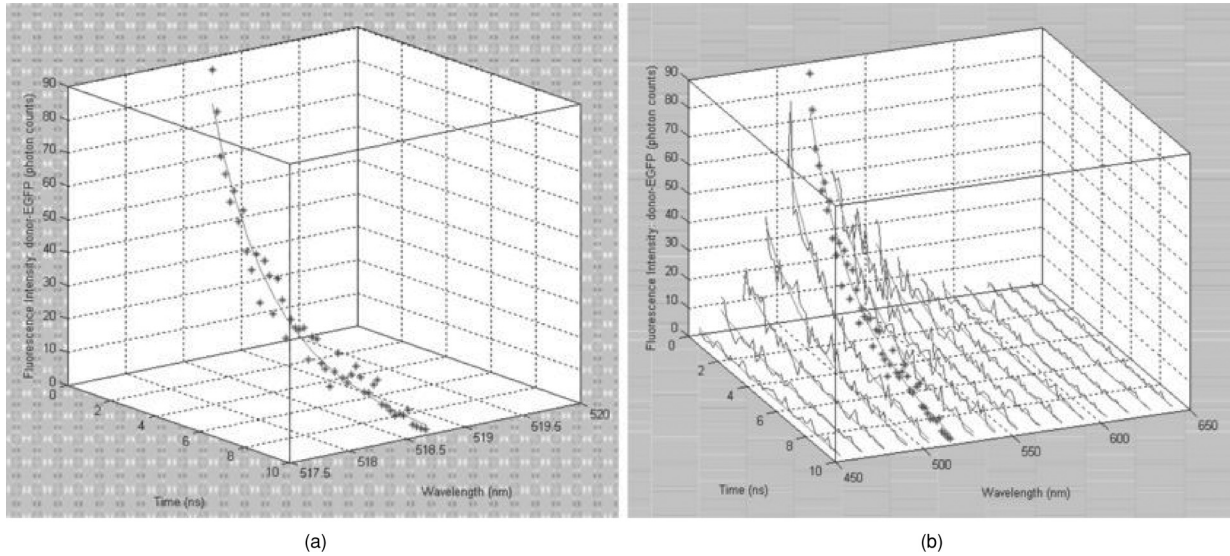


Fig. 4 A monoexponential donor model for N2A cells transfected with EGFP alone: (a) single channel fitting between 525 and 512.5nm, and (b) global fitting between 450 and 650 nm over 16 channels.

When fixing the donor amplitudes or the acceptor amplitudes during the multispectral global fit with a monoexponential donor-acceptor model, the value for the goodness of fit measure becomes worse. This suggests that the amplitude coefficients for the donor or acceptor when they are alone are not identical to the ones when donor and acceptor are in proximity. This could be because the separation of amplitudes is not always possible (i.e., for when the signals are not entirely linearly independent), or some other background is involved, such as acceptor bleed-through, autofluorescence, or acceptor bleaching. The signal coming from the donor is of higher intensity, thus overwhelming the signal coming from the acceptor.

The FRET efficiency results are consistent across the case scenarios where all the involved amplitudes and decay rates were variable parameters for the fitting routine and for the case scenarios where only the donor and acceptor amplitudes were considered variable parameters, whereas the donor decay rates were kept constant throughout the fitting procedure. When trying

to keep the amplitudes at fixed values for either the donor or the acceptor species, the measure for the goodness of fit becomes worse and the FRET efficiency loses consistency.

In a second approximation, a two-exponential profile is assumed for the donor. Table 13 shows the results for when assuming a two-exponential donor model for a donor in the presence of the acceptor as given by Eq. (12) and the corresponding time-dependent concentration of the acceptor as given by Eq. (13).

Figure 5 illustrates the results for globally fitting the 16 channels donor-acceptor EGFP-mRFP data with a one-exponential donor model [Fig. 5(a)] and a two-exponential donor model [Fig. 5(b)]. It can be seen that the fitting profiles for a two-exponential donor [as shown in Fig. 5(b)] have a curvature at time zero, especially between 650 and 550 nm.

Figure 6 shows the amplitudes for the donor and acceptor from the global fitting over 16 channels when using a two-exponential donor-acceptor model and: (i) freely fitting all the donor and acceptor amplitudes and decay rates or (ii) keeping

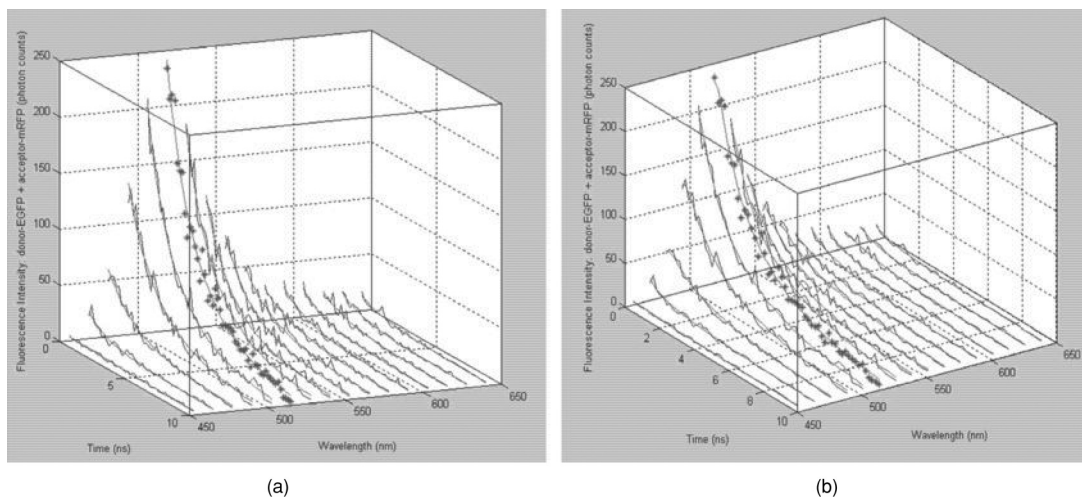


Fig. 5 Global fitting between 450 and 650 nm for donor-acceptor EGFP-mRFP over 16 channels, using (a) a monoexponential donor-acceptor model and (b) a two-exponential donor-acceptor model.

Table 1 Decay rates and lifetimes for donor-EGFP alone (derived from a cell transfected only with EGFP) from single-channel data.

Single-channel fitting, using a one-exponential donor model with free-fitting donor amplitude and decay rates.

Sample name	Channel (wavelength range)	Parameter name	Fitted parameter value	Goodness of fit χ^2 statistic
Donor-EGFP	11 (525–512.5 nm)	D_0	72.0744	1.57
		K_f^D	0.16	
		K_{rl}^D	0.25	
		τ^D lifetime of donor	2.42 ns	

Table 2 Decay rates and lifetimes for donor-EGFP alone (derived from a cell transfected only with EGFP) from single-channel data.

Global fitting, 11 channels, using a one-exponential donor model with free-fitting donor amplitudes and decay rates.

Sample name	Channel (wavelength range)	Parameter name	Fitted parameter value	Goodness of fit χ^2 statistic
Donor-EGFP	4–14 (612.5–475 nm)	D_0	72.0565	1.78
		K_f^D	0.1433	
		K_{rl}^D	0.2434	
		τ^D lifetime of donor	2.6 ns	

Table 3 Decay rates and lifetimes for donor-EGFP alone (derived from a cell transfected only with EGFP) from single-channel data.

Global fitting, 16 channels, using a one-exponential donor model with free-fitting donor amplitudes and decay rates.

Sample name	Channel (wavelength range)	Parameter name	Fitted parameter value	Goodness of fit χ^2 statistic
Donor-EGFP	1–16 (650–450 nm)	D_0	72.0618	2.7
		K_f^D	0.1458	
		K_{rl}^D	0.2406	
		τ^D lifetime of donor	2.6 ns	

Table 4 Decay rates and lifetimes for donor-acceptor: EGFP-mRFP sample (derived from a cell transfected with the tandem EGFP-mRFP) from single-channel data.

Single-channel fitting, using a donor-acceptor model assuming a one-exponential behavior of the donor, with free fitting for donor and acceptor amplitudes and decay rates.

Sample name	Channel (wavelength range)	Parameter name	Fitted parameter value	Goodness of fit χ^2 statistic
Donor-EGFP + acceptor-mRFP	11 (525–512.5 nm)	D_0	180.6134	1.7266
		K_f^D	0.2286	
		K_{rl}^D	0.2286	
		K_{ET}^D	0.3732	
		K_f^A	0.1671	
		K_{rl}^A	0.1910	
		τ^{DA} lifetime of donor with acceptor present	1.2 ns	
FRET efficiency	50% (if $\tau^D \sim 2.42$ ns)			

Table 5 Decay rates and lifetimes for donor-acceptor: EGFP-mRFP sample (derived from a cell transfected with the tandem EGFP-mRFP) from single-channel data.

Single-channel fitting, using a donor-acceptor model, assuming a one-exponential behavior of the donor with fixed donor amplitudes and decay rates (from Table 1) and free fitting for acceptor amplitudes and decay rates.

Sample name	Channel (wavelength range)	Parameter name	Fitted parameter value	Goodness of fit χ^2 statistic
donor-EGFP + acceptor-mRFP	11 (525–512.5 nm)	D_0	229.9008	1.87
		K_f^D	Fixed 0.16 (from Table 1)	
		K_{rl}^D	Fixed 0.25 (from Table 1)	
		K_{ET}^D	0.2479	
		K_f^A	0.1859	
		K_{rl}^A	1.0173	
		τ^{DA} lifetime of donor with acceptor present	1.5 ns	
FRET efficiency	38% (if $\tau^D \sim 2.42$ ns)			

the donor amplitudes and decay rates constant and free fitting only the acceptor amplitudes and decay rates or (iii) keeping the donor decay rates constant and free fitting the donor amplitudes and the acceptor amplitudes and decay rates. When the donor amplitudes were kept constant, they were kept constant to the values shown in Fig. 6 for the donor-EGFP alone.

The lifetime of the donor alone was obtained using a mono-exponential fit for the N2A cells transfected only with EGFP; the value obtained in this way is $\tau^D = 2.5$ ns. The lifetime of the disturbed donor was obtained using a two-exponential model for the fit performed on N2A cells transfected with EGFP and mRFP. As shown in Table 16, the FRET-ing donor lifetime is

$\tau^{DA} = 0.9$ ns. Figure 7 shows the results from the Becker and Hickl fit when using a two-exponential donor model.

As shown in Tables 1–16, the donor lifetime values for the donor in the presence of the acceptor are shorter than the values for the donor lifetime in the absence of the acceptor in both fitting procedures (i.e., with one- and two-exponential models) regardless whether the donor parameters are constant or variable. The values for the goodness of fit are better (closer to 1) when using a two-exponential donor-acceptor model. The χ^2 value is further away from the value of 1 for a monoexponential donor model. This would suggest that the donor in the presence of the acceptor shows a two-exponential decay profile. Also, the

Table 6 Decay rates and lifetimes for donor-acceptor: EGFP-mRFP sample (derived from a cell transfected with the tandem EGFP-mRFP) from single-channel data.

Single-channel (channel 11) fitting, using a donor-acceptor model, assuming a one-exponential behavior of the donor with fixed donor decay rates (from Table 1) and free fitting for donor and acceptor amplitudes and acceptor decay rates.

Sample name	Channel (wavelength range)	Parameter name	Fitted parameter value	Goodness of fit χ^2 statistic
Donor-EGFP + acceptor-mRFP	11 (525–512.5 nm)	D_0	206.6	1.64
		K_f^D	Fixed 0.16 (from Table 1)	
		K_{rl}^D	Fixed 0.25 (from Table 1)	
		K_{ET}^D	0.4178	
		K_f^A	0.2715	
		K_{rl}^A	0.0862	
		τ^{DA} lifetime of donor with acceptor present	1.2 ns	
FRET efficiency	50% (if $\tau^D \sim 2.42$ ns)			

Table 7 Decay rates and lifetime values for donor-acceptor: EGFP-mRFP sample (derived from a cell transfected with the tandem EGFP-mRFP) from 11 channels of data.

Global fitting, 11 channels, using a donor-acceptor model, assuming a one-exponential behavior of the donor with free fitting for donor and acceptor amplitudes and decay rates.

Sample name	Channel (wavelength range)	Parameter name	Fitted parameter value	Goodness of fit χ^2 statistic
Donor-EGFP + acceptor-mRFP	4–14 (612.5 – 475 nm)	D_0	124.5601	1.2952
		K_f^D	0.1748	
		K_{rl}^D	0.2631	
		K_{ET}^D	0.3652	
		K_f^A	0.1766	
		K_{rl}^A	0.1766	
		τ^{DA} lifetime of donor with acceptor present	1.24 ns	
FRET efficiency		48.8% (if $\tau^D \sim 2.42$ ns)		

value for K_2^D is similar to the value for $K_f^D + K_{rl}^D$, which consolidates the proof that the signal coming from the donor is a mixture of signals coming from the “FRET-ing” and “non-FRET-ing” donors.

To test the applicability of global analysis for a relevant biological question and to compare it to conventional methods, we analyzed cells transfected with GGA1-EGFP or cotransfected with GGA1-EGFP plus BACE-mRFP to confirm protein proximity in living cells. We already proved the two-exponential donor model was the best suited for data analysis of the disturbed donor, and Table 17 shows the results for the donor alone

given by Eq. (3) (with $K_{ET} = 0$), and Tables 17–20 show the results for the donor-acceptor model, with the “disturbed” donor as given by Eq. (12) (with $K_2^D = K_f^D + K_{rl}^D$) and the corresponding time-dependent concentration of the acceptor as given by Eq. (13).

Tables 21–23 show the results when using the Becker and Hickl software for fitting the data in the classical FLIM approach that uses a two-exponential model for the donor. When free fitting the data from the donor-acceptor: GGA1-EGFP plus BACE-mRFP sample with the two-exponential model for the donor, the longer donor lifetime was retrieved with a value

Table 8 Decay rates and lifetime values for donor-acceptor: EGFP-mRFP sample (derived from a cell transfected with the tandem EGFP-mRFP) from 11 channels of data.

Global fitting 11 channels, using a donor-acceptor model, assuming a one-exponential behavior of the donor with fixed donor-only decay rates and free fitting for donor and acceptor amplitudes and acceptor decay rates.

Sample name	Channel (wavelength range)	Parameter name	Fitted parameter value	Goodness of fit χ^2 statistic
Donor-EGFP + acceptor-mRFP	4–14 (612.5–475 nm)	D_0	114.2681	2.5796
		K_f^D	Fixed 0.16 (from Table 1)	
		K_{rl}^D	Fixed 0.25 (from Table 1)	
		K_{ET}^D	0.3976	
		K_f^A	0.1770	
		K_{rl}^A	0.1770	
		τ^{DA} lifetime of donor with acceptor present	1.24 ns	
FRET efficiency		48.8% (if $\tau^D \sim 2.42$ ns)		

Table 9 Decay rates and lifetime values for donor-acceptor : EGFP-mRFP sample (derived from a cell transfected with the tandem EGFP-mRFP) from 16 channels of data.

Global fitting, 16 channels, using a donor-acceptor model, assuming a one-exponential behavior of the donor with free-fitting donor and acceptor amplitudes and donor and acceptor decay rates.

Sample name	Channel (wavelength range)	Parameter name	Fitted parameter value	Goodness of fit χ^2 statistic
Donor-EGFP + acceptor-mRFP	1–16 (650–450 nm)	D_0	181.3258	2.56
		K_f^D	0.2989	
		K_{rl}^D	0.3763	
		K_{ET}^D	0.1437	
		K_f^A	0.1778	
		K_{rl}^A	0.1778	
		τ^{DA} lifetime of donor with acceptor present	1.22 ns	
FRET efficiency			49.5% (if $\tau^D \sim 2.42$ ns)	

Table 10 Decay rates and lifetime values for donor-acceptor: EGFP-mRFP sample (derived from a cell transfected with the tandem EGFP-mRFP) from 16 channels of data.

Global fitting, 16 channels, using a donor-acceptor model, assuming a one-exponential behavior of the donor with fixed donor-only decay rates and free-fitting donor and acceptor amplitudes and acceptor decay rates.

Sample name	Channel (wavelength range)	Parameter name	Fitted parameter value	Goodness of fit χ^2 statistic
Donor-EGFP + acceptor-mRFP	1–16 (650–450 nm)	D_0	159.3411	2.55
		K_f^D	Fixed 0.16 (from Table 1)	
		K_{rl}^D	Fixed 0.25 (from Table 1)	
		K_{ET}^D	0.4103	
		K_f^A	0.1780	
		K_{rl}^A	0.1780	
		τ^{DA} lifetime of donor with acceptor present	1.21 ns	
FRET efficiency			50.3% (if $\tau^D \sim 2.42$ ns)	

Table 11 Decay rates and lifetime values for donor-acceptor: EGFP-mRFP sample (derived from a cell transfected with the tandem EGFP-mRFP) from 16 channels of data.

Global fitting, 16 channels, using a donor-acceptor model, assuming a one-exponential behavior of the donor with free-fitting donor amplitudes and acceptor decay rates, fixed donor-only decay rates, and fixed acceptor amplitudes to a value of zero (channels 8–16).

Sample name	Channel (wavelength range)	Parameter name	Fitted parameter value	Goodness of fit χ^2 statistic
Donor-EGFP + acceptor-mRFP	1–16 (650–450 nm)	D_0	140.3101	3.2
		K_f^D	Fixed 0.16 (from Table 1)	
		K_{rl}^D	Fixed 0.25 (from Table 1)	
		K_{ET}^D	0.0331	
		K_f^A	0.0644	
		K_{rl}^A	0.0920	
		τ^{DA} lifetime of donor with acceptor present	2.27 ns	
FRET efficiency			6% (if $\tau^D \sim 2.42$ ns)	

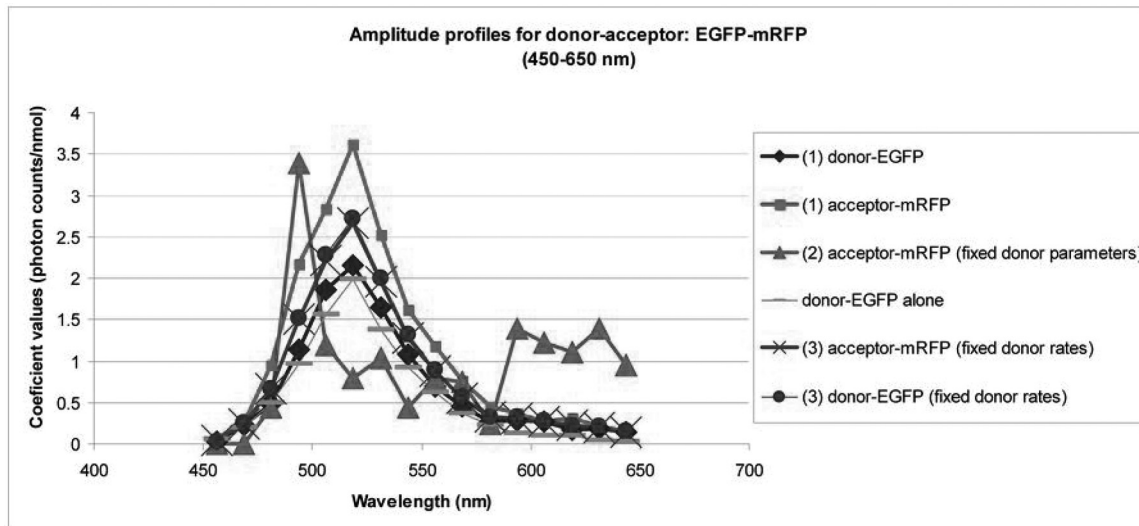


Fig. 6 Amplitude coefficient values for donor-EGFP alone, and donor-acceptor: EGFP-mRFP (derived from an N2A cell transfected only with EGFP and with the tandem EGFP-mRFP, respectively) from a global fitting over 16 channels (from channel 1 to channel 16) using a two-exponential donor model.

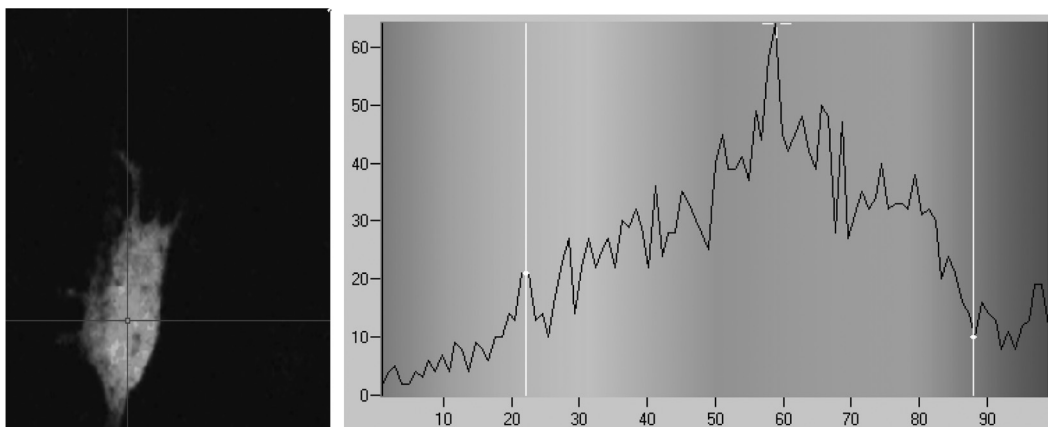


Fig. 7 FRET efficiency histogram from N2A cells transfected with EGFP and mRFP, fitted with a two-exponential donor model.

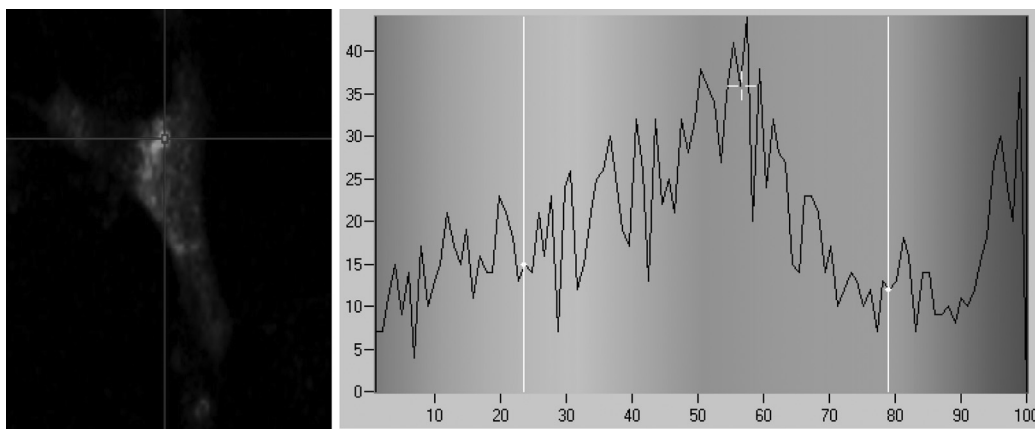


Fig. 8 FRET efficiency histogram from data corresponding to N2A cells transfected with GGA1-EGFP and BACE-mRFP, fitted with a two-exponential donor model, fixed donor lifetime in the presence of the acceptor to $\tau^{DA} = 1.5$ ns.

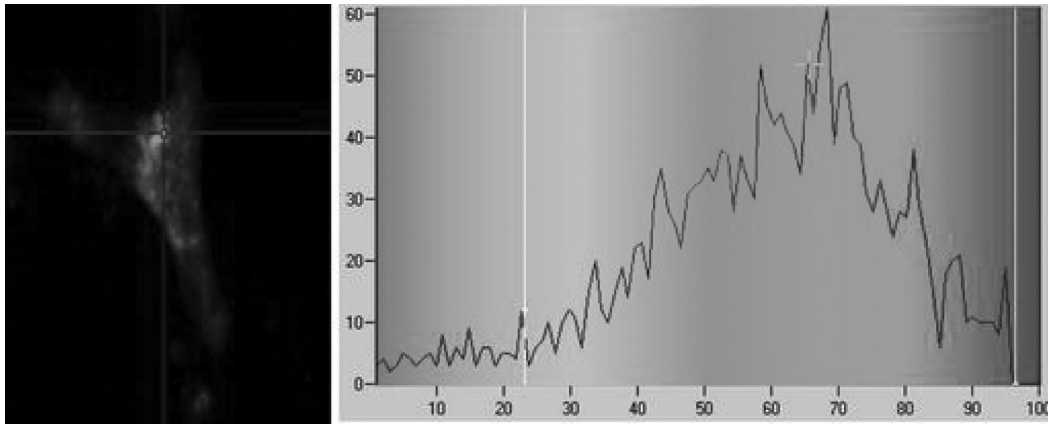


Fig. 9 FRET efficiency histogram from data corresponding to from N2A cells transfected with GGA1-EGFP and BACE-mRFP, fitted with a two-exponential donor model, fixed donor lifetime in the absence of the acceptor to $\tau^D = 2.7$ ns.

Table 12 Decay rates and lifetime values for donor-acceptor: EGFP-mRFP sample (derived from a cell transfected with the tandem EGFP-mRFP) from 16 channels of data.

Global fitting, 16 channels, using a donor-acceptor model, assuming a one-exponential behavior of the donor with free-fitting acceptor amplitudes and acceptor decay rates, and fixed donor decay rates and donor amplitudes.

Sample name	Channel (wavelength range)	Parameter name	Fitted parameter value	Goodness of fit χ^2 statistic
Donor-EGFP + acceptor-mRFP	1-16 (650 – 450 nm)	D_0	258.6702	3.45
		K_f^D	Fixed 0.16 (from Table 1)	
		K_{rl}^D	Fixed 0.25 (from Table 1)	
		K_{ET}^D	1.85	
		K_f^A	0.2120	
		K_{rl}^A	0.2120	
		τ^{DA} lifetime of donor with acceptor present	0.44 ns	
		FRET efficiency	81% (if $\tau^D \sim 2.42$ ns)	

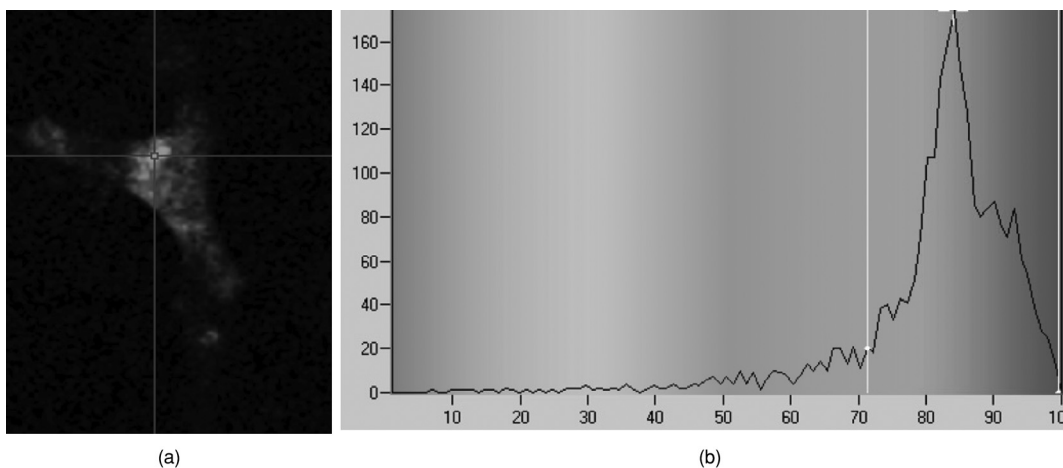


Fig. 10 FRET efficiency histogram from N2A cells transfected with GGA1-EGFP and BACE-mRFP, fitted with a two-exponential donor model, fixed donor lifetime in the presence of the acceptor to $\tau^{DA} = 0.4$ ns.

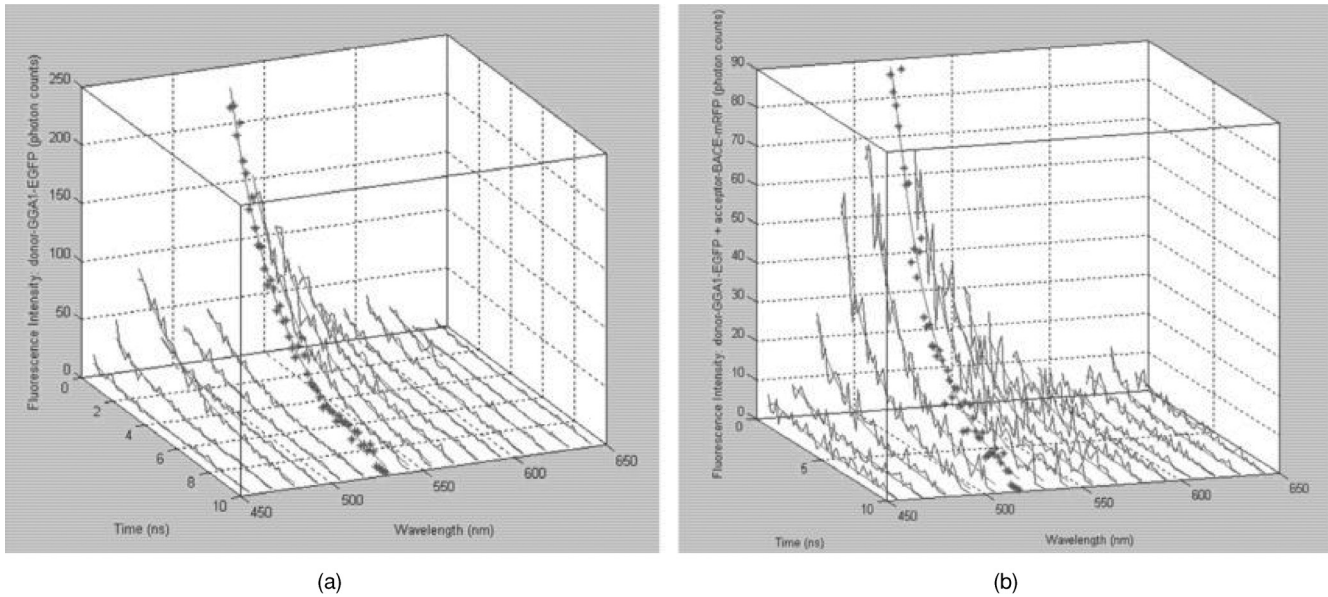


Fig. 11 Global fitting between 450 and 650 nm using a (a) one-exponential donor model for donor-GGA1-EGFP and (b) two-exponential donor-acceptor model for donor-GGA1-EGFP plus acceptor-BACE-mRFP.

of $\tau^D \sim 2.4$ ns across the whole sample. The shorter donor lifetime (corresponding to the donor found in proximity of the acceptor) was found to be of $\tau^{DA} = 1.5$ ns.

Performing a fit for the donor-acceptor data with two-exponential donor model, but with a fixed value for the donor lifetime (in the presence of the acceptor) of $\tau^{DA} = 1.5$ ns, obtained a donor lifetime value of $\tau^D = 2.7$ ns as shown in Table 21 and illustrated in Fig. 8.

When performing a fit for the donor-acceptor data with the two-exponential donor model, but with a fixed value for the donor lifetime (in the absence of the acceptor) of $\tau^D = 2.7$ ns, retrieves a donor lifetime value of $\tau^{DA} = 1.2$ ns as shown in Table 22 and illustrated in Fig. 9.

Performing a fit for the donor-acceptor data with the two-exponential donor model, but with a fixed value for the donor

lifetime (in the presence of the acceptor) of $\tau^{DA} = 0.4$ ns (which is coincident to the result obtained by the global analysis as shown in Table 18), retrieved a value for the donor lifetime of $\tau^D = 2.3$ ns as shown in Table 24 and illustrated in Fig. 10.

It can be seen from Table 18 that the FRET efficiency for the interaction between GGA1-EGFP and BACE-mRFP is higher ($\sim 84\%$) when fitting all the parameters for both donor and acceptor, as opposed to keeping the donor's amplitudes and/or decay rates constant. The χ^2 measure for the goodness of fit is however slightly better when fitting all the parameters as opposed to keeping some donor parameters constant. Nevertheless, when keeping all the donor amplitudes and decay rates or only the decay rates constant, the FRET efficiency values are comparable to values of $\sim 38\%$, as shown in Tables 19 and 20. Figure 11 shows the profiles for the donor-GGA1-EGFP alone

Table 13 Decay rates and donor lifetime values for donor-acceptor: EGFP-mRFP sample, globally fitted over all 16 channels, assuming a two-exponential behavior of the donor.

Global fitting, 16 channels, using a donor-acceptor model, assuming a two-exponential behavior of the donor with free-fitting donor and acceptor amplitudes and decay rates.

Sample name	Channel (wavelength range)	Parameter name	Fitted parameter value	Goodness of fit χ^2 statistic
Donor-EGFP + acceptor-mRFP	1–16 (650–450 nm)	D_0	163.9504	1.3
		K_f^D	0.6597	
		K_{rl}^D	0.6597	
		K_{ET}^D	3.0389	
		K_2^D	1.32	
		K_f^A	0.1842	
		K_{rl}^A	0.1842	
		τ^{DA} donor lifetime with acceptor present	0.22 ns	
FRET efficiency			91.5% (if $\tau^D \sim 2.6$ ns)	

Table 14 Decay rates and donor lifetime values for a donor-acceptor: EGFP-mRFP sample, globally fitted over all 16 channels, assuming a two-exponential behavior of the donor.

Global fitting, 16 channels, using a donor-acceptor model, assuming a two-exponential behavior of the donor with free-fitting acceptor amplitudes and decay rates and fixed donor amplitudes and decay rates (from Table 1).

Sample name	Channel (wavelength range)	Parameter name	Fitted parameter value	Goodness of fit χ^2 statistic
donor-EGFP + acceptor-mRFP	1–16 (650–450 nm)	D_0	123.6468	1.6971
		K_f^D	Fixed 0.16 (from Table 1)	
		K_{rl}^D	Fixed 0.25 (from Table 1)	
		K_2^D	0.3139	
		K_{ET}^D	0.4164	
		K_f^A	2.0334	
		K_{rl}^A	2.0334	
		τ^{DA} donor lifetime with acceptor present	1.2 ns	
		FRET efficiency	53.4% (if $\tau^D \sim 2.6$ ns)	

Table 15 Decay rates and donor lifetime values for a donor-acceptor: EGFP-mRFP sample, globally fitted over all 16 channels, assuming a two-exponential behavior of the donor.

Global fitting, 16 channels, using a donor-acceptor model, assuming a two-exponential behavior of the donor with free-fitting donor and acceptor amplitudes, free-fitting acceptor decay rates, and fixed donor decay rates (from Table 1).

Sample name	Channel (wavelength range)	Parameter name	Fitted parameter value	Goodness of fit χ^2 statistic
Donor-EGFP + acceptor-mRFP	1–16 (650–450 nm)	D_0	88	1.27
		K_f^D	Fixed 0.16 (from Table 1)	
		K_{rl}^D	Fixed 0.25 (from Table 1)	
		K_2^D	0.41	
		K_{ET}^D	0.3426	
		K_f^A	0.2027	
		K_{rl}^A	0.2027	
		τ^{DA} donor lifetime with acceptor present	1.3 ns	
		FRET efficiency	48.9% (if $\tau^D \sim 2.6$ ns)	

Table 16 Decay rates and donor lifetime values for donor-acceptor: EGFP-mRFP sample, single-channel fitting, assuming a two-exponential behavior of the donor.

Becker and Hickl software: Single-channel fitting, using two-exponential donor model.

Sample name	Channel (wavelength range)	Parameter name	Fitted parameter value	Goodness of fit χ^2 statistic
donor-EGFP + acceptor-mRFP	11 (525–512.5 nm)	τ^D donor lifetime without acceptor	2.5 ns	1.33
		τ^{DA} donor lifetime with acceptor present	0.9 ns	
		FRET efficiency	57% (with $\tau^D \sim 2.6$ ns)	

Table 17 Decay rates and donor lifetime values for donor: GGA1-EGFP sample, globally fitted over all 16 channels, assuming a one-exponential behavior of the donor.

Global fitting, 16 channels, using a one-exponential donor model with free fitting of donor and amplitudes and decay rates.

Sample name	Channel (wavelength range)	Parameter name	Fitted parameter value	Goodness of fit χ^2 statistic
Donor-GGA1-EGFP	1–16 (650–450 nm)	D_0	51.6585	1.4427
		K_f^D	0.15	
		K_{rl}^D	0.22	
		τ^D donor lifetime with no acceptor	2.66 ns	

Table 18 Decay rates and donor lifetime values for donor-acceptor: GGA1-EGFP plus BACE-mRFP sample, globally fitted over 16 channels, assuming a two-exponential behavior of the donor.

Global fitting, 16 channels, using a donor-acceptor model, assuming a two-exponential behavior of the donor with free fitting for donor and acceptor amplitudes and decay rates.

Sample name	Channel (wavelength range)	Parameter name	Fitted parameter value	Goodness of fit χ^2 statistic
Donor-GGA1-EGFP + acceptor-BACE-mRFP	1–16 (650–450 nm)	D_0	58.8011	1.5406
		K_f^D	0.495	
		K_{rl}^D	0.495	
		K_{ET}^D	1.5260	
		K_f^A	0.1746	
		K_{rl}^A	0.1746	
		τ^{DA} donor lifetime with acceptor present	0.39 ns	
FRET efficiency	85 = % (if $\tau^D \sim 2.66$ ns)			

Table 19 Decay rates and donor lifetime values for donor-acceptor: GGA1-EGFP plus BACE-mRFP sample, globally fitted over 16 channels, assuming a two-exponential behavior of the donor.

Global fitting, 16 channels, using a donor-acceptor model, assuming a two-exponential behavior of the donor with fixed donor amplitudes and decay rates (from Table 17) and free-fitting acceptor amplitudes and decay rates.

Sample name	Channel (wavelength range)	Parameter name	Fitted parameter value	Goodness of fit χ^2 statistic
Donor-GGA1-EGFP + acceptor-BACE-mRFP	1–16 (650–450 nm)	D_0	40.8589	1.6488
		K_f^D	Fixed 0.15 (from Table 17)	
		K_{rl}^D	Fixed 0.22 (from Table 17)	
		K_{ET}^D	0.2500	
		K_f^A	0.1251	
		K_{rl}^A	0.1167	
		τ^{DA} donor lifetime with acceptor present	1.6 ns	
FRET efficiency	38% (if $\tau^D \sim 2.66$ ns)			

Table 20 Decay rates and donor lifetime values for donor-acceptor: GGA1-EGFP plus BACE-mRFP sample, globally fitted over 16 channels, assuming a two-exponential behavior of the donor.

Global fitting, 16 channels, using a donor-acceptor model, assuming a two-exponential behavior of the donor with fixed donor decay rates (from Table 17) and free-fitting donor and acceptor amplitudes and acceptor decay rates.

Sample name	Channel (wavelength range)	Parameter name	Fitted parameter value	Goodness of fit χ^2 statistic
donor-GGA1-EGFP + acceptor-BACE-mRFP	1–16 (65–450 nm)	D_0	30.4945	1.5724
		K_f^D	Fixed 0.15 (from Table 17)	
		K_{rl}^D	Fixed 0.22 (from Table 17)	
		K_{ET}^D	0.6471	
		K_f^A	0.1593	
		K_{rl}^A	0.2115	
		τ^{DA} donor lifetime with acceptor present	0.98 ns	
		FRET efficiency	37.6% (if $\tau^D \sim 2.66$ ns)	

and the donor-acceptor GGA1-EGFP and BACE-mRFP for all 16 channels, using a one-exponential model for the donor alone and a two-exponential donor for the donor-acceptor model.

Figures 8–10 show the results from the FRET efficiency calculations using the Becker and Hickl software with a donor model using two exponentials. As shown in Tables 22 and 23, the values for the average FRET efficiency and the FRET efficiency calculated from one pixel are in higher agreement for when fixing the shorter donor lifetime (in the presence of the acceptor) to the value obtained by the global analysis. The histogram for the FRET efficiency calculated in this manner has a higher S/N ratio, as illustrated in Fig. 10 and Table 23.

Figure 12 shows the amplitudes for the donor and acceptor from the global fitting over 16 channels when using a two-exponential donor-acceptor model and (i) freely fitting all the donor and acceptor amplitudes and decay rates or (ii) keeping the donor decay rates constant and free fitting the donor amplitudes and the acceptor amplitudes and decay rates.

The amplitudes for the donor GGA1-EGFP alone are different from the amplitudes of the disturbed donor as shown in Fig. 12. This could be because, when the donor and acceptor

are in close proximity to each other, their FRET interaction is strongly coupled or the donor's contribution to the signal is more complex than assumed in this paper.

4 Discussion and Conclusions

The retrieval of the decay rates using a global minimization routine over multiple channels offers the advantage of increased data volume, thus possibly higher information content. The lifetime of the donor in the presence of the acceptor was, in all cases, shorter, as expected due to the nonfluorescent energy transfer from the donor to the acceptor that contributes to the decaying number of donors in the initial excited state. Two different assumptions were made in the fitting routine: first, a monoexponential behavior of the donor and, second, a two-exponential behavior of the donor. The global fit was better when assuming a two-exponential decay for the donor molecules. This model is in better agreement to the distribution of the donor and of the acceptor molecules in the sample: not all the acceptor and donor molecules are close enough to each other in order for the FRET interaction to take place. Only those donor molecules

Table 21 Donor lifetime values for donor-acceptor: GGA1-EGFP plus BACE-mRFP sample, fitted over one channel, assuming a two-exponential behavior of the donor.

Becker and Hickl software: single channel fitting, using two-exponential donor model with free-fitting donor lifetimes in the absence of the acceptor and fixed donor lifetime in the presence of the acceptor.

Sample name	Channel (wavelength range)	Parameter name	Fitted parameter value	Goodness of fit χ^2 statistic
Donor-GGA1-EGFP + acceptor-BACE-mRFP	11 (525–512.5 nm)	τ^D donor lifetime in absence of acceptor	2.7 ns	1.14
		τ^{DA} donor lifetime in presence of acceptor	Fixed 1.5 ns	
		Average FRET efficiency	65%	
		FRET efficiency from 1 pixel	45%	

Table 22 Donor lifetime values for donor-acceptor: GGA1-EGFP plus BACE-mRFP sample, fitted over one channel, assuming a two-exponential behavior of the donor.

Becker and Hickl software: single-channel fitting, using two-exponential donor model with fixed donor lifetimes in the absence of the acceptor and free-fitting donor lifetime in the presence of the acceptor.

Sample name	Channel (wavelength range)	Parameter name	Fitted parameter value	Goodness of fit χ^2 statistic
Donor-GGA1-EGFP + acceptor-BACE-mRFP	11 (525–512.5 nm)	τ^D donor lifetime in absence of acceptor	Fixed 2.7 ns	1.12
		τ^{DA} donor lifetime in presence of acceptor	1.2 ns	
		Average FRET efficiency	57%	
		FRET efficiency from 1 pixel	38%	

Table 23 Donor lifetime values for donor-acceptor: GGA1-EGFP plus BACE-mRFP sample, fitted over one channel, assuming a two-exponential behavior of the donor.

Becker and Hickl software: single channel (11) fitting, using the two-exponential donor model with free-fitting donor lifetimes in the absence of the acceptor and fixed donor lifetime in the presence of the acceptor.

Sample name	Channel (wavelength range)	Parameter name	Fitted parameter value	Goodness of fit χ^2 statistic
Donor-GGA1-EGFP + acceptor-BACE-mRFP	11 (525–512.5 nm)	τ^D donor lifetime in absence of acceptor	2.3 ns	1.11
		τ^{DA} donor lifetime in presence of acceptor	Fixed 0.4 ns (from Table 18)	
		Average FRET efficiency	84%	
		FRET efficiency from 1 pixel	82%	

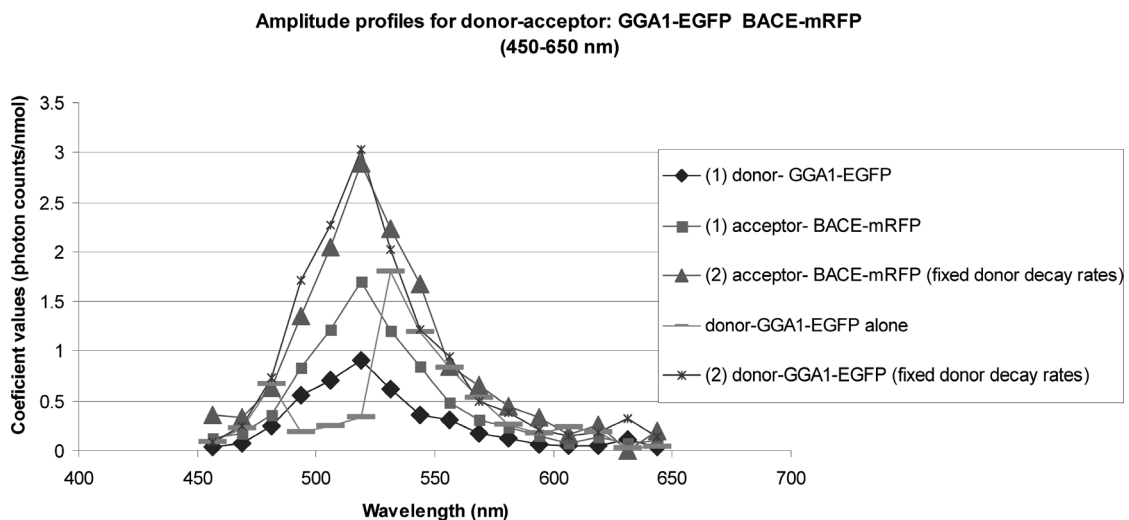


Fig. 12 Amplitude profiles for donor-GGA1-EGFP and donor-GGA1-EGFP plus acceptor-BACE mRFP obtained for a donor-acceptor model, with a two-exponential donor.

close enough to the acceptor molecules are able to transfer their energy to them via FRET.

For the donor model made by N2A cells transfected with the donor-EGFP, the χ^2 measure for the goodness of fit is better (its value is closer to 1) when only considering the data from stronger intensity channel(s) as shown in Tables 1–3. The best fitting was obtained, in this case, from single-channel fitting [(i.e., channel 11), see Table 1], where EGFP emits the strongest fluorescence intensity signal. In this case, the data from the different spectral channels might not be linearly independent, thus bringing in data from more channels might not enhance the information content. The donor lifetime is the same for all the different spectral channels.

When the acceptor molecules are present for the model made by N2A cells cotransfected with the tandem donor-EGFP-acceptor-mRFP, different channels can have different intensity signals coming from the donors and from the acceptors. In this case, multispectral data may be linearly independent and analyzing it globally across all the channels could have richer information content than from a single channel. For a single-channel donor-acceptor analysis (channel 11), the χ^2 values are comparable (see Tables 4–6). When performing the global analysis on the channels with a higher S/N ratio (channels 4–14) with free fitting for the donor and acceptor amplitudes and decay rates, the χ^2 measure for the goodness of fit has a value closer to 1 (see Table 7, which shows that the model and the experimental data are in closer agreement).

Table 8 shows the results from globally fitting the same 11 channels (channel 4–14), but with fixed donor-only decay rates and free fitting for the donor and acceptor amplitudes and acceptor decay rates. In this case, even though the value of the χ^2 measure for the goodness of fit is not as good as in Table 7, the retrieved donor decay rates and FRET efficiency are comparable in value to the ones in Table 7.

Tables 9–12 show the results for when performing a globally fitting routine for donor-EGFP with acceptor-mRFP over 16 channels (channel 1–16), with different fixed donor parameters.

From Tables 9 and 10, it can be seen that the best fit is obtained when freely fitting all the donor and acceptor amplitudes and decay rates or when fixing only the donor decay rates, with free fitting for the donor and acceptor amplitudes and acceptor decay rates. In these two cases, the values for the donor lifetime in the presence of the acceptor have similar values of ~ 1.2 ns, as well as the FRET efficiency values of $\sim 50\%$.

Table 11 shows the results for globally fitting all 16 channels, but with fixed amplitudes for the acceptor (at zero values) on the channels where the acceptor did not fluoresce in isolation—the values for the fluorescent profile of mRFP alone was taken from literature.²³ Table 12 shows the results for globally fitting the same 16 channels with fixed amplitudes and decay rates for the donor to the values obtained from the global analysis of the donor alone over all 16 channels. In both cases, the χ^2 measure for the goodness of fit exhibits a value farther away from 1, which is an indicator of the model not being appropriate for the experimental data. Also, the values obtained for the lifetime of the donor in the presence of the acceptor are dissimilar in Tables 11 and 12, along with the values obtained for the FRET efficiency calculations. These results could confirm the hypothesis that the donor and acceptor have a strongly coupled dipole-dipole interaction that changes their emission profiles when they are in proximity to

each other, from when they are in isolation. These results could also highlight the fact that the donor's contribution to the signal is more complex than assumed in this paper.

When the donor-acceptor model for the EGFP-mRFP sample assumes a two-exponential behavior of the donor, with free-fitting parameters for the donor and acceptor amplitudes and decay rates, the lifetime of the donor in the presence of the acceptor has a value of ~ 0.22 ns with a FRET efficiency of $\sim 91.5\%$, as shown in Table 13 and Fig. 5(b). Table 14 shows the results for a global fitting routine performed over all 16 channels using a donor-acceptor model with a two-exponential behavior of the donor and fixed donor amplitudes and decay rates to the values obtained from the global fit of the donor in isolation. The value for the lifetime of the disturbed donor of ~ 1.2 ns, along with the value for the FRET efficiency of $\sim 53\%$, are in agreement with the values obtained in Tables 9 and 10. The χ^2 measure for the goodness of fit from Table 14 is slightly worse than the value in Table 13. However, as shown in Table 15, when performing the global fitting routine over all 16 channels with a two-exponential donor model, with fixed donor decay rates (to the values from Table 1), the χ^2 measure for the goodness of fit is the best in Table 15 and the closest to 1. Again, the lifetime of the donor in the presence of the acceptor is of ~ 1.3 ns with a FRET efficiency of $\sim 49\%$. These values are comparable to the values obtained in Tables 7–10, although the χ^2 measure for the goodness of fit has the best value in Table 15. The global analysis using a two-exponential donor for a donor-acceptor model gives the best estimation for the donor-EGFP-acceptor-mRFP experimental data. When using the Becker and Hickl software for performing the classical FLIM analysis on one channel only, with a two-exponential model, the lifetime of the donor in the presence of the acceptor is of ~ 0.9 ns with a FRET efficiency of $\sim 57\%$, as shown in Table 16 and illustrated in Fig. 7.

For the donor-GGA1-EGFP plus acceptor-BACE-mRFP sample, the 16 channels fitting routine for a donor-acceptor model using a two-exponential model for the donors gives a value for the donor lifetime of ~ 0.39 ns with FRET efficiency of $\sim 85\%$ when fitting all the donor parameters, as shown in Table 17. On the other hand, when performing a global fitting routine over 16 channels while keeping the donor parameters constant, the two-exponential model for the donors gives a donor lifetime of 1.6 ns with a FRET efficiency of $\sim 38\%$, as shown in Table 18. This is in accordance to the donor lifetime (when only the donor decay rates are constant) which is ~ 0.98 ns with a FRET efficiency of $\sim 37.6\%$, as shown in Table 19. However, the value for the goodness of fit measure is better when the fitting routine minimizes all the amplitudes from the donor and acceptor, as opposed to keeping some of them constant. This is an indicator that the spectra profile of both the donor and acceptor might change when they interact via dipole-dipole coupling, which introduces a change in their emission spectra from the case when they are observed in isolation. The donor molecules that transfer their energy to the acceptor molecules via FRET interaction will have a weaker fluorescence signal than the donor molecules that do not interact via FRET. However, because of the dipole-dipole interaction during FRET, the electron clouds belonging to the donor and to the acceptor can change shape during the resonant beat. This change can affect the emission spectrum of the donor, as well as the emission spectrum of the acceptor.

All the presented results conclude that the behavior of the donors in the presence of the acceptor molecules is two exponential. The work presented in this paper considered the signals measured by 1 pixel only on all the detectors that were emitted by the donor molecules as well as the acceptor molecules. In comparison, Laptanok *et al.*²⁰ described the quantitative determination of FRET in live cells using the rise time of acceptor fluorescence as determined with FLIM, using the information from all the pixels, from one detector only.

In future work, considering only the signals from the “rising time” of the acceptor will give a better estimation of the FRET efficiency because this is the signal triggered by the resonant transfer of energy only.

The S/N ratio is not always better for more channels. If some of the channels used are “noisier,” then the overall data might have a lower S/N average value. The measure for the goodness of fit is worsened with the decrease of the S/N ratio. In a FRET experiment where autofluorescence occurs additionally, the S/N ratio is worsened by the autofluorescence that overlaps the FRET signal. However, the donor and the acceptor molecules can have different fluorescence profiles on the different spectral regions that are analyzed. Acknowledging that a signal from both the donor and acceptor are detected simultaneously and reflecting this in the mathematics of the global analysis can give, overall, a more accurate parameter estimation of the data.

Acknowledgments

We thank Jonas Pervaiz, a student from the Hochschule Aalen, who invested a lot of effort to build a user friendly graphical user interface for the global analysis. This work was carried out with financial support by the Ministry of Research and Development of Germany, order FKZ: Grant Nos. 13N9240 and 13N11179, the Ministry of Economic Affairs of Germany, order IGF-Nr: Grant Nos. 15727 N/1 and BMWi VII A5-4042 40/7; and a grant from the Alzheimer Forschungsinstitut (AFI) e.V. to C. v. A.

References

1. T. Förster, “Zwischenmolekulare Energiewanderung und Fluoreszenz,” *Ann. Phys.* **437**(2), 55–75 (1948).
2. A. Grinvald, E. Haas, and I. Z. Steinberg, “Evaluation of the distribution of distances between energy donors and acceptors by fluorescence decay,” *Proc. Natl. Acad. Sci. USA* **69**(8), 2273–2277 (1972).
3. B. Schuler, E. A. Lipman, and W. A. Eaton, “Probing the free-energy surface for protein folding with single-molecule fluorescence spectroscopy,” *Nature* **419**(6908), 743–747 (2002).
4. B. J. Bacskai, J. Skoch, G. A. Hickey, R. Allen, and B. T. Hyman, “Fluorescence resonance energy transfer determinations using multiphoton fluorescence lifetime imaging microscopy to characterize amyloid-beta plaques,” *J. Biomed. Opt.* **8**(3), 368–375 (2003).
5. O. Berezovska, B. J. Bacskai, and B. T. Hyman, “Monitoring proteins in intact cells,” *Sci. Aging Knowledge Environ.* **2003**(23), PE14 (2003).
6. C. A. von Arnim, M. M. Tangredi, I. D. Peltan, B. M. Lee, M. C. Irizarry, A. Kinoshita, and B. T. Hyman, “Demonstration of BACE (beta-secretase) phosphorylation and its interaction with GGA1 in cells by fluorescence-lifetime imaging microscopy,” *J. Cell Sci.* **117**(Pt 22), 5437–5445 (2004).
7. C. A. von Arnim, R. Spoelgen, I. D. Peltan, M. Deng, S. Courchesne, M. Koker, T. Matsui, H. Kowa, S. F. Lichtenthaler, M. C. Irizarry, and B. T. Hyman, “GGA1 acts as a spatial switch altering amyloid precursor protein trafficking and processing,” *J. Neurosci.* **26**(39), 9913–9922 (2006).
8. B. von Einem, D. Schwanzar, F. Rehn, A. S. Beyer, P. Weber, M. Wagner, H. Schneckenburger, and C. A. von Arnim, “The role of low-density receptor-related protein 1 (LRP1) as a competitive substrate of the amyloid precursor protein (APP) for BACE1,” *Exp. Neurol.* **225**(1), 85–93 (2010).
9. D. J. Chorvat and A. Chorvatova, “Multi-wavelength fluorescence lifetime spectroscopy: a new approach to the study of endogenous fluorescence in living cells and tissues,” *Laser Phys. Lett.* **6**(3), 175–193 (2009).
10. K. C. Benny Lee, J. Siegel, S. E. D. Webb, S. Lévêque-Fort, M. J. Cole, R. Jones, K. Dowling, M. J. Lever, and P. M. W. French, “Application of the stretched exponential function to fluorescence lifetime imaging,” *Biophys. J.* **81**(3), 1265–1274 (2001).
11. A. Periasamy and R. M. Clegg, *FLIM Microscopy in Biology and Medicine*, CRC Press, Taylor & Francis Group LLC, Boca Raton (2010).
12. Q. S. Hanley, D. J. Arndt-Jovin and T. M. Jovin, “Spectrally resolved fluorescence lifetime imaging microscopy,” *Appl. Spectrosc.* **56**(2), 155–166 (2002).
13. D. K. Bird, K. W. Eliceiri, C. H. Fan, and J. G. White, “Simultaneous two-photon spectral and lifetime fluorescence microscopy,” *Appl. Opt.* **43**(27), 5173–5182 (2004).
14. A. Ruck, C. Hulshoff, I. Kinzler, W. Becker, and R. Steiner, “SLIM: a new method for molecular imaging,” *Microsc. Res. Tech.* **70**(5), 485–492 (2007).
15. A. Rück, F. Dolp, R. Steiner, C. Steinmetz, B. von Einem, and C. A. F. von Arnim, “SLIM for multispectral FRET imaging,” *Proc. SPIE* **6860**, 68601F (2008).
16. J. M. Beechem, “Global analysis of biochemical and biophysical data,” *Methods Enzymol.* **210**, 37–54 (1992).
17. M. R. Otto, M. P. Lillo, and J. M. Beechem, “Resolution of multiphase reactions by the combination of fluorescence total-intensity and anisotropy stopped-flow kinetic experiments,” *Biophys. J.* **67**(6), 2511–2521 (1994).
18. S. Laptanok, K. M. Mullen, J. W. Borst, I. H. M. van Stokkum, V. V. Apanasovich, and A. J. W. G. Visser, “Fluorescence lifetime imaging microscopy (FLIM) data analysis with TIMP,” *J. Stat. Softw.* **18**(8), 1–20 (2007).
19. P. J. Verveer, A. Squire, and P. I. Bastiaens, “Global analysis of fluorescence lifetime imaging microscopy data,” *Biophys. J.* **78**(4), 2127–2137 (2000).
20. S. P. Laptanok, J. W. Borst, K. M. Mullen, I. H. van Stokkum, A. J. Visser, and H. van Amerongen, “Global analysis of Förster resonance energy transfer in live cells measured by fluorescence lifetime imaging microscopy exploiting the rise time of acceptor fluorescence,” *Phys. Chem. Chem. Phys.* **12**(27), 7593–7602 (2010).
21. H. E. Grecco, P. Roda-Navarro, and P. J. Verveer, “Global analysis of time correlated single photon counting FRET-FLIM data,” *Opt. Express* **17**(8), 6493–6508 (2009).
22. W. Becker, *Advanced Time-Correlated Single Photon Counting Techniques*, Springer Series in Chem. Phys., Springer-Verlag, Berlin (2005).
23. R. E. Campbell, O. Tour, A. E. Palmer, P. A. Steinbach, G. S. Baird, D. A. Zacharias, and R. Y. Tsien, “A monomeric red fluorescent protein,” *Proc. Natl. Acad. Sci. USA* **99**(12), 7877–7882 (2002).
24. C. A. von Arnim, B. von Einem, P. Weber, M. Wagner, D. Schwanzar, R. Spoelgen, W. L. Strauss, and H. Schneckenburger, “Impact of cholesterol level upon APP and BACE proximity and APP cleavage,” *Biochem. Biophys. Res. Commun.* **370**(2), 207–212 (2008).